Available online at www.sciencedirect.com

SciVerse ScienceDirect

Proceedings of the Combustion Institute 34 (2013) 2707–2717

Proceedings of the Combustion Institute

www.elsevier.com/locate/proci

Cup-burner flame structure and extinguishment by CF_3Br and C_2HF_5 in microgravity

Fumiaki Takahashi [a,*], Viswanath R. Katta [b], Gregory T. Linteris [c], Oliver C. Meier [d]

[a] Case Western Reserve University, Cleveland, OH 44106, USA
[b] Innovative Scientific Solutions, Inc., Dayton, OH 45440, USA
[c] National Institute of Standards and Technology, Gaithersburg, MD 20899, USA
[d] The Boeing Company, Seattle, WA 98124, USA

Available online 27 September 2012

Abstract

The effects of fire-extinguishing agents CF_3Br and C_2HF_5 on the structure and extinguishing processes of microgravity cup-burner flames have been studied numerically. Propane and a propane–ethanol–water fuel mixture, prescribed for a Federal Aviation Administration (FAA) aerosol can explosion simulator test, were used as the fuel. The time-dependent, two-dimensional numerical code, which includes a detailed kinetic model (177 species and 2986 reactions), diffusive transport, and a gray-gas radiation model, revealed unique flame structure and predicted the minimum extinguishing concentration of agent when added to the air stream. The peak reactivity spot (i.e., reaction kernel) at the flame base stabilized a trailing flame. The calculated flame temperature along the trailing flame decreased downstream due to radiative cooling, causing local extinction at <1250 K and flame tip opening. As the mole fraction of agent in the coflow (X_a) was increased gradually: (1) the *premixed*-like reaction kernel weakened (i.e., lower heat release rate) (but nonetheless formed at higher temperature); (2) the flame base stabilized increasingly higher above the burner rim, parallel to the axis, until finally blowoff-type extinguishment occurred; (3) the calculated maximum flame temperature remained at nearly constant (≈1700 K) or mildly increased; and (4) the total heat release of the entire flame decreased (inhibited) for CF_3Br but increased (enhanced) for C_2HF_5. In the lifted flame base with added C_2HF_5, H_2O (formed from hydrocarbon-O_2 combustion) was converted further to HF and CF_2O through exothermic reactions, thus enhancing the heat-release rate peak. In the trailing flame, "two-zone" flame structure developed: CO_2 and CF_2O were formed primarily in the inner and outer zones, respectively, while HF was formed in both zones. As a result, the unusual (non-chain branching) reactions and the combustion enhancement (increased total heat release) due to the C_2HF_5 addition occurred primarily in the trailing *diffusion* flame.

Keywords: Aircraft cargo-bay fire suppression; Halon replacement HFC-125; Diffusion flame stabilization; Reaction kernel; Microgravity combustion

* Corresponding author. Address: Case Western Reserve University, c/o National Center for Space Exploration Research, NASA Glenn Research Center, MS 110-3, 21000 Brookpark Road, Cleveland, OH 44135, USA. Fax: +1 216 433 3793.
E-mail addresses: fxt13@case.edu, fumiaki.takahashi-1@nasa.gov (F. Takahashi).

1. Introduction

Because of its destruction of stratospheric ozone, the use of the effective fire suppressant CF_3Br (bromotrifluoromethane, Halon 1301) has

1540-7489/$ - see front matter © 2012 The Combustion Institute. Published by Elsevier Inc. All rights reserved.
http://dx.doi.org/10.1016/j.proci.2012.06.091

been discontinued, with exceptions being certain critical applications such as the suppression of cargo-bay fires in aircraft. Recently, some Halon replacement agents, including C_2HF_5 (pentafluoroethane, HFC-125), have been evaluated in a mandated Federal Aviation Administration (FAA) test [1,2], in which a simulated explosion of an aerosol can, caused by a fire, must be suppressed by the agent. Unfortunately, unlike CF_3Br, the other agents, when added at approximately one-half their inerting concentrations, created a higher over-pressure in the test chamber and thus failed the test.

Similar combustion enhancement by various halogenated inhibitors has been described in other experiments for certain conditions: high-speed turbulent flames [3], constant-volume closed-vessel combustion device (bomb) [4], and shock tubes [5,6]. Mawhinney et al. [7] found that unwanted accelerated burning could be caused by application of water mist to a fire (due to fluid-dynamic enhancement of the burning). Hamins et al. [8] reviewed previous work on enhanced burning with application of fire suppressants, and also concluded that the enhanced combustion was due to more rapid mixing of fuel vapor with air, from the combined effects of enhanced turbulent mixing and more vigorous liquid fuel atomization from agent jet impingement. In other tests, halogenated hydrocarbons added to the air stream of diffusion flames have been shown to increase total heat release. Holmstedt et al. [9] reported that HFC 227ea or HFC 134a added to the fuel (propane) stream of a turbulent jet burner increased the total heat release, by a factor of 2 and 3.8, respectively, for concentrations just below that required for extinguishment of the flame. The present authors [10] also found that CF_3H added to the oxidizer stream in a methane cup-burner flame increased the total heat release.

Recent work [11,12] employing thermodynamic equilibrium and perfectly stirred-reactor calculations (for premixed systems) indicated that higher overpressures in the FAA aerosol can tests might be due to higher heat release from reaction of the inhibitor itself. Nonetheless, the agents should still reduce the overall reaction rate and inhibit the reaction [13,14]. For diffusion flames, however, the flame structure and inhibition or combustion enhancement processes are not yet fully understood. By using comprehensive numerical simulations, this paper extends previous work [15–21] on cup-burner flames to more realistic fuels (propane and the FAA aerosol can test [ACT] fuel mixture) and fire-extinguishing agents. Only zero-gravity ($0g_n$) results are presented in this paper to uncover previously unknown, essential physical and chemical processes in a relatively calm environment. The earth-gravity ($1g_n$) results obtained by the present unsteady calculations, revealing more dynamic nature (the flame-base oscillations [18] followed by premature blowoff [21]), will be reported elsewhere.

2. Computational method

A time-dependent, axisymmetric numerical code (UNICORN) [22,23] is used for the simulation of coflow diffusion flames stabilized on the cup burner. The code solves the axial and radial (z and r) full Navier–Stokes momentum equations, continuity equation, and enthalpy- and species-conservation equations on a staggered-grid system. A clustered mesh system is employed to trace the gradients in flow variables near the flame surface. The thermo-physical properties such as enthalpy, viscosity, thermal conductivity, and binary molecular diffusion of all of the species are calculated from the polynomial curve fits developed for the temperature range 300 to 5000 K. Mixture viscosity and thermal conductivity are then estimated using the Wilke and Kee expressions, respectively. Molecular diffusion is assumed to be of the binary-diffusion type, and the diffusion velocity of a species is calculated using Fick's law and the effective-diffusion coefficient of that species in the mixture. A simple radiation model based on the optically thin-media assumption was incorporated into the energy equation. Only radiation from CH_4, CO, CO_2, and H_2O was considered in the present study. The finite-difference forms of the momentum equations are obtained using an implicit QUICKEST scheme [22], and those of the species and energy equations are obtained using a hybrid scheme of upwind and central differencing.

A comprehensive reaction mechanism was assembled, for the simulation of propane or ACT fuel flames with CF_3Br or C_2HF_5 added to air, based on the four-carbon hydrocarbon mechanism of Wang and co-workers [24,25] (111 species and 1566 one-way elementary reactions), detailed reactions of ethanol (5 species and 72 reactions) by Dryer and co-workers [26–28], the bromine parts of the mechanism of Babushok et al. [29,30] (10 additional species and 148 reactions), and a subset (51 species and 1200 reactions) of NIST HFC starting mechanism [31,32]. The final chemical kinetics model (177 species, 2986 reactions) is integrated into the UNICORN code. Transport data for 139 species are available in the literature; for the remaining 38 species, data are constructed through matching these species with the nearest species (based on molecular weight) with known transport data. The fuel is propane or the ACT fuel gas mixture (volume fractions: C_3H_8, 0.159; C_2H_5OH, 0.454; and H_2O, 0.387), and the agent is CF_3Br or C_2HF_5 added to "air" (21 % O_2 in N_2).

The boundary conditions are treated in the same way as that reported in earlier papers

[15–21]. The computational domain is bounded by the axis of symmetry, a chimney wall, and the inflow and outflow boundaries. The burner outer diameter is 28 mm and the chimney inner diameter is 95 mm. The burner wall (1-mm long and 1-mm thick tube) temperature is set at 600 K and the wall surface is under the no-slip velocity condition. The mean fuel velocity is 0.307 cm/s for propane or 0.853 cm/s for the ACT fuel, and the mean oxidizer velocity is 10.7 cm/s at 294 K.

Validation of the code with the kinetic model was performed through the simulation of opposing-jet diffusion flames. The predicted extinction strain rates for propane–air flames (no agent) were within 7.5% of the measured values (with an error margin of 9%) by Zegers et al. [33]. The predicted extinction agent concentrations for CF_3Br and C_2HF_5 are within 4% of the measured concentrations in weakly stretched flames and within 25% in highly stretched flames.

3. Results and discussion

3.1. Internal flame structure

The flame-base region supports a trailing flame and controls the flame attachment and detachment processes [34]. Small variations in the agent mole fraction in the coflowing oxidizing stream (X_a) result in profound changes near the extinguishment limit. Figure 1 shows the calculated structure of a $0g_n$ near-limit propane flame with agent (C_2HF_5) added at $X_a = 0.093$. The variables include the velocity vectors ($\mathbf{v}$), isotherms (T), and heat-release rate ($\dot{q}$). The flame base is already detached and lifted above the burner rim. The contours of the heat-release rate showed a peak reactivity spot (i.e., the *reaction kernel* [34]) at the height from the burner rim, $z_k = 10.9$ mm. The chain radical species (H, O, and OH), as well as heat, diffused back against the incoming flow at the flame base (edge), thus promoting vigorous reactions to form the reaction kernel. The values of the variables at the reaction kernel were $\dot{q}_k = 76\ \mathrm{W/cm^3}$, $|\mathbf{v}_k| = 0.164$ m/s, $T_k = 1600$ K, $X_{O_2,k} = 0.026$, and $-\hat{\omega}_{O_2,k} = 0.000095\ \mathrm{mol/cm^3\ s}$; where $X_{O_2,k}$ and $-\hat{\omega}_{O_2,k}$ are the mole fraction and consumption rate of oxygen, respectively. The fuel-oxidizer-agent mixing time (t_{mix}), determined by dividing the reaction kernel standoff distance ($z_k = 10.9$ mm) by the mean oxidizer velocity ($U_{ox} = 10.7$ cm/s), was 100 ms. The reaction kernel broadened laterally, supporting a trailing flame with two-zone structure to be described later.

Figure 2 shows the radial and axial variations of the species mole fractions (X_i), temperature, and heat-release rate (HRR) crossing the reaction kernel of the propane flame with C_2HF_5 added at $X_a = 0.093$. There are striking differences (as well as similarities) in the radial plot at $z = 10.9$ mm (Fig. 2a), compared to typical chemically passive agent (CO_2, N_2, Ar, and He) cases for methane flames [20,21]; i.e., X_{CO} was much larger, X_{H_2O} was much smaller, and there are broad and large

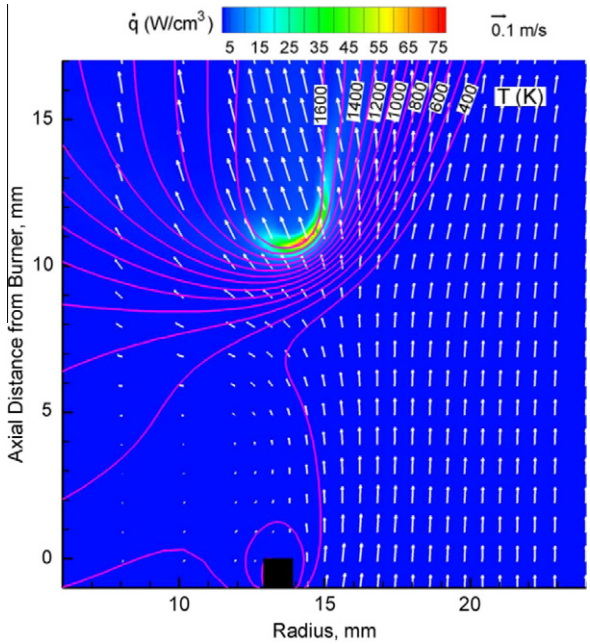

Fig. 1. Calculated structure of a $0g_n$ propane flame in air with added C_2HF_5 at $X_a = 0.093$.

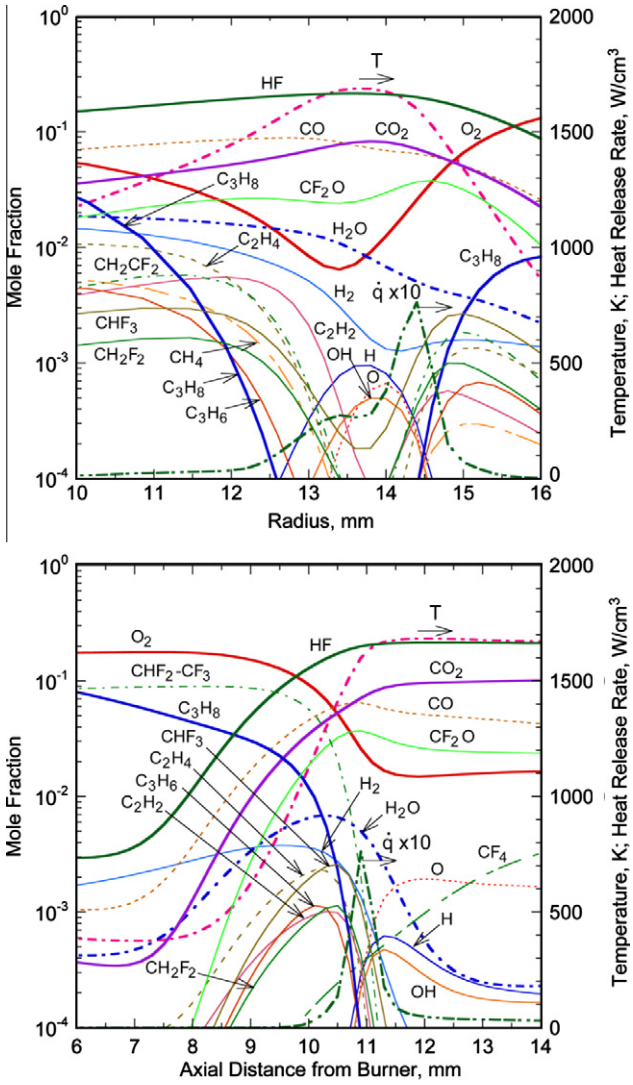

Fig. 2. Calculated structure through the reaction kernel for a $0g_n$ propane flame in air with C_2HF_5 at $X_a = 0.093$. (a) Radial ($z = 10.9$ mm) and (b) axial ($r = 14.4$ mm) variations of the mole fractions, temperature, and total heat-release rate.

concentrations of HF, CF_2O, and minor fluorinated intermediates on both fuel and oxidizer sides. The heat-release rate peak was formed on the oxidizer side. The axial plot (Fig. 2b) revealed the premixed-like nature of the unique flame-base structure. At increasing axial distances along $r = 14.4$ mm, the mole fractions of the reactants (C_3H_8, O_2, and C_2HF_5) decreased, intermediate species and chain radials (H, O, and OH) peaked, the temperature increased, the heat-release rate peaked, and the final products (CO_2, HF, and CF_2O) were formed. Surprisingly, H_2O and H_2 formed by hydrocarbon-O_2 reaction were completely converted to HF and CF_2O. Also notice that X_O was much higher than X_H and X_{OH}. The reactions of HF and CF_2O formation contributed most, by a large measure, to the overall reaction rate and heat-release rate at the reaction kernel (to be shown later).

Figure 3 shows the radial variations of calculated variables crossing the trailing flame at $z = 15.9$ mm ($z_k + 5$ mm). At this height, the flame is characterized by "two-zone" structure (inner and outer) as is evident from two heat-release rate peaks. In the inner zone (11 mm $< r <$ 15 mm), T, X_H, X_O, and X_{OH} peaked, and hydrocarbon fuel fragments and, more importantly X_{H_2O} and X_{H_2} from the fuel side, diminished, unlike in a neat diffusion flame without a halogenated agent [21]. As the case at the reaction kernel, X_O peak was much

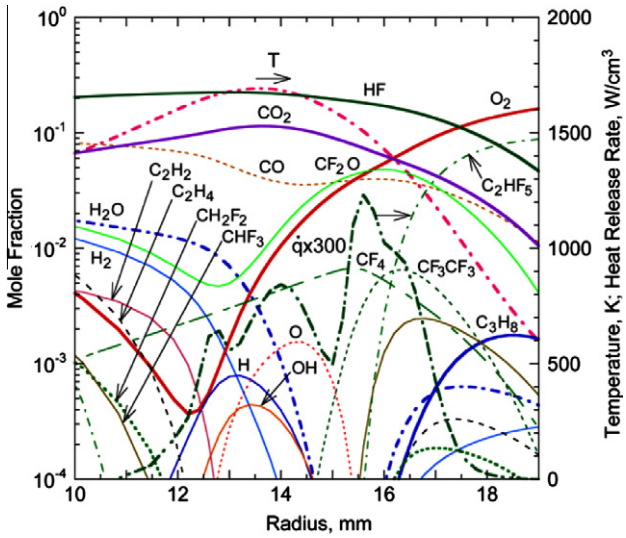

Fig. 3. Calculated radial variations of the mole fractions, temperature, and total heat-release rate through the trailing flame for a $0g_n$ propane flame in air with C_2HF_5 at $X_a = 0.093$ ($z_k = 15.9$ mm).

larger than X_H and X_{OH}. In the outer zone (15 mm $< r <$ 18 mm), the agent (C_2HF_5) from the air side decomposed and diminished, the mole fractions of many fluorinated species (CF_2O, CF_4, CF_3–CF_3, CHF_3, etc.) peaked, and, interestingly, there were no chain radicals (H, O, and OH). Small mole fractions of C_3H_8, leaked over the flame-base standoff distance, and H_2O were observed on the air side. Figure 4 shows the radial variations of the calculated production (+) or consumption (−) rates (Fig. 4a) and heat-release rates (Fig. 4b) of species i crossing the trailing flame at $z = 15.9$ mm. In the inner zone, H_2, H_2O, CO, O_2, F, and CF_2O were consumed, HF and CO_2 were formed, and the chain radicals (H, O, and OH) were formed and consumed depending on the radial location. In the outer zone, C_2HF_5 and O_2 were consumed, HF, CF_2O, and CO were formed, and F was formed on the fuel side and consumed on the air side. The major contributors to the overall heat-release rate (Fig. 4b) were the formation of CO_2 and HF in the inner zone and CF_2O and HF in the outer zone.

Figure 5 shows the maximum heat-release rate of each elementary step crossing the reaction kernel and the trailing flame ($z = 10.9$ mm and 15.9 mm, respectively). At the reaction kernel (red), a number of steps for CF_2O and HF (and CO_2) formation by radical attack (both chain radicals [OH, O, and H] and the free F atom) on various fluorinated fragments contributed to overall HRR. In the trailing flame (blue), the main HRR contributors depended on the location; (inner zone): the F-attack on H_2O and H_2 to form HF in addition to the ordinary CO + OH → CO_2 conversion; and (outer zone): the F-attack on C_2HF_5 to form HF and the O-attack on CF_3 to form CF_2O.

The structure of the ACT fuel flame (not shown) was very similar to that of the propane flame, except for generally larger X_{H_2O} and $X_{C_2H_5OH}$, and smaller $X_{C_3H_8}$ because of the initial fuel composition.

3.2. Blowoff extinguishment mechanisms

In previous papers [20,21], the blowoff-type extinguishment processes of methane cup-burner flames were investigated using chemically passive agents (CO_2, N_2, He, and Ar). There are both common and different features with chemically active agents (CF_3Br and C_2HF_5) described below. Figure 6 shows the effects of the agent volume fraction in the coflowing oxidizer on the calculated axial (z_k) and radial (r_k) positions of the reaction kernel from the burner exit on the axis in both propane and the ACT fuel. In the present unsteady calculations, as X_a was increased incrementally, the flame-stabilizing reaction kernel moved downstream gradually and then more steeply as the extinguishment limit approached ($X_a > 0.02$ for CF_3Br, $X_a > 0.08$ for C_2HF_5). For each X_a, a stable stationary flame was obtained. The radial location of the reaction kernel remained nearly constant over a wide range of X_a and increased slightly as it lifted off, thereby more premixing occurred over the standoff distance. The calculated minimum extinguishing concentrations (MECs) of CF_3Br were $X_a = 0.0254$ and 0.0208 for propane and the ACT fuel, respectively, and those of C_2HF_5 were $X_a = 0.097$ and 0.112 for propane and the ACT fuel, respectively. There is no $0g_n$ experimental data

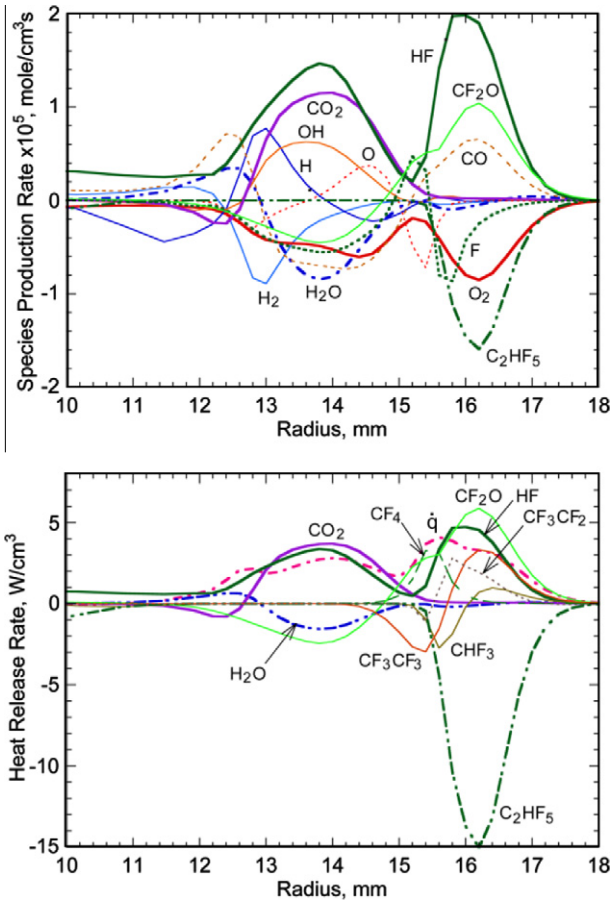

Fig. 4. Calculated radial variations of the (a) species production rates, and (b) species and total heat-release rates through the trailing flame for a $0g_n$ propane flame in air with C_2HF_5 at $X_a = 0.093$ ($z_k = 15.9$ mm).

for these fuels available for comparison. Measured MEC values for propane flames in $1g_n$ are $X_a = 0.028$ to 0.043 for CF_3Br and ≈0.103 for C_2HF_5 [35–37].

Figure 7 shows the calculated temperature and heat-release rate along the propane flame zone for various X_a approaching the extinguishing limit. The vigorously burning flame base represented by the peak $\dot{q}$ (reaction kernel) sustained stationary combustion processes in the flow and held the order-of-magnitude weaker (smaller $\dot{q}$) trailing flame zone downstream. The peak heat-release rate values (70 to 80) W/cm^3 in the near-limit propane flames were the same as the methane flames with a chemically passive agent (CO_2 [20], N_2, He, or Ar [21]). The flame temperature peaked around 1700 K, decreased linearly downstream due to radiative heat loss, whereupon the exothermic reactions shut off, causing flame-tip opening, around 1200 to 1250 K (see dashed lines).

Figure 8 shows the variations of the temperature and velocity components along a vertical path crossing the reaction kernel of propane flames. For each X_a value of added C_2HF_5, and proceeding up the vertical path from $z = 0$: (1) the temperature rises steeply as the flame base is approached; (2) the axial velocity (U) first decreases toward the flame base (due to stream-tube expansion into the wake region and around the flame base), then increases downstream due to longitudinal gas expansion at high temperatures. As X_a was increased, the magnitude of the radial component decreased. For the near-limit X_a (0.093 to 0.094) and the sufficiently long mixing time (0.1 to 0.2 s), the minimum axial velocity component just before the temperature rise was ≈0.05 m/s, which was comparable to the methane-chemically passive agent cases (≈0.07 m/s) [20,21].

It was found previously [20,21] for methane flames with added N_2 or CO_2 that the calculated incoming flow velocity (≈0.07 m/s) into the near-limit flame base was nearly the same as the laminar flame speeds (0.07 to 0.1 m/s) at corresponding

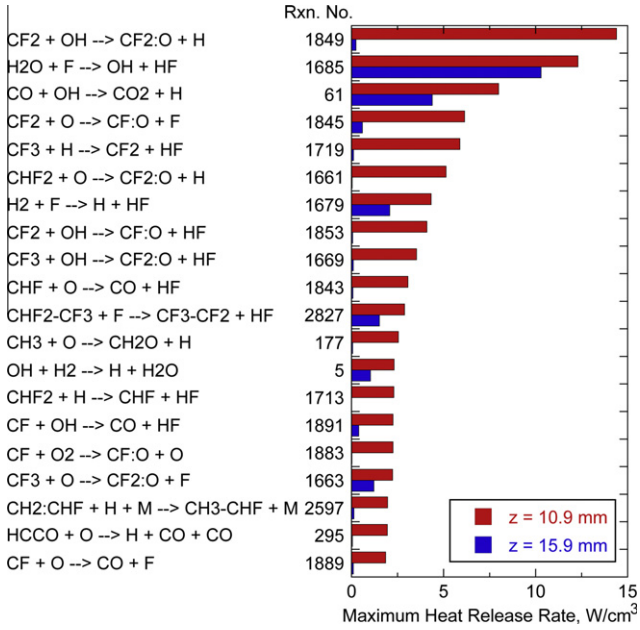

Fig. 5. Maximum heat-release rate of each step across the reaction kernel and trailing flame for a $0g_n$ C_3H_8 flame in air with C_2HF_5 at $X_a = 0.093$.

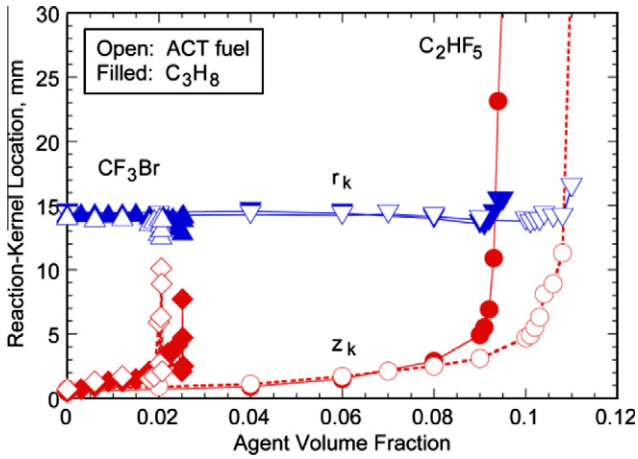

Fig. 6. Calculated reaction kernel coordinates of $0g_n$ propane and ACT fuel flames in air with added agent.

dilution, consistent with a classic view [38] of diffusion flame stabilization. For various C_1–C_3 hydrocarbons, it was also found [39] that the calculated transit speed of a diffusion flame base (edge), which propagated through the near-stagnant stratified mixing layer, equaled each fuel's stoichiometric laminar flame speed, available in the literature. Similar calculations were performed recently (not shown) for both propane and the ACT fuel using the present kinetic model. The calculated diffusion flame edge transit velocity was 0.06 m/s for both propane and the ACT fuel at X_a value of added C_2HF_5 of 0.10 and 0.11, respectively, which were close to the calculated blowoff limit conditions ($X_a = 0.097$ and 0.112, respectively). It was also noticed that as the concentration of added C_2HF_5 was increased to $X_a > 0.06$, the flame edge transit velocity for the ACT fuel became greater than that of pure propane. This result was consistent with the present result that the ACT fuel flame was more stable at large X_a and the MEC was greater than that of propane.

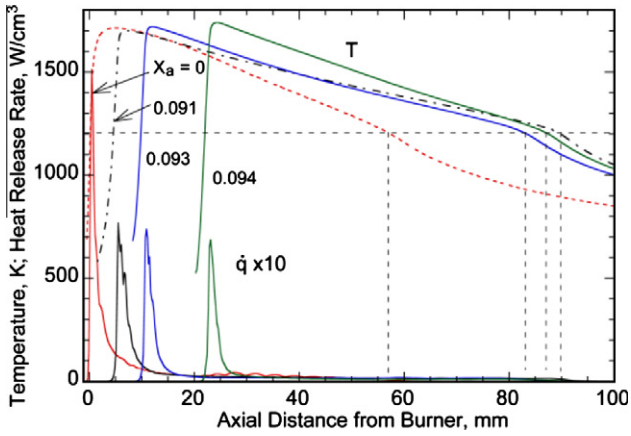

Fig. 7. Calculated temperature and heat-release rate along the flame zone in $0g_n$ propane flames in air with or without added C_2HF_5.

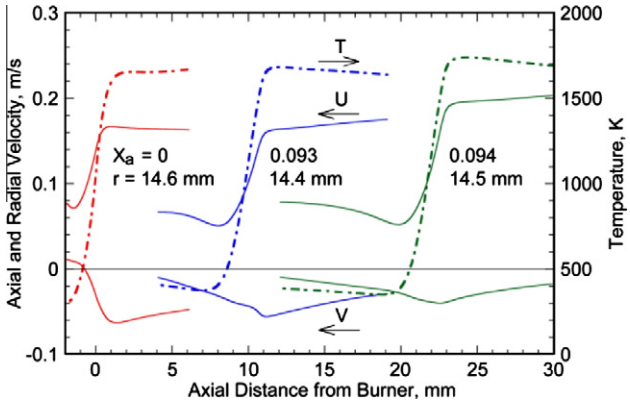

Fig. 8. Axial variations of the calculated axial and radial velocity components and temperature crossing the reaction kernel of $0g_n$ propane flames in air with added C_2HF_5.

The incoming flow velocity around the flame base is important in diffusion flame stability as it represents the reciprocal of the residence time through the reaction kernel. Figure 9 shows the effects of the agent volume fraction in the oxidizer on the calculated total ($|\mathbf{v}_k|$), axial (U_k), and radial velocity (V_k) at the reaction kernel. For both fuels and both agents, as X_a was increased, the absolute values of $|\mathbf{v}_k|$ initially increased, decreased generally to a minimum, and then increased steeply as the flame lifted off. Figure 10 shows the temperature, heat-release rate, and a ratio of the heat-release rate and the total velocity at the reaction kernel. For both fuels and both agents, as X_a was increased, the reaction kernel weakened (lower heat-release rate), but the flame stabilized at higher temperature at a location which provided a larger reaction time (lower $|\mathbf{v}_k|$). There is a striking difference compared with the passively acting agents for which the T_k was nearly constant [20,21]. Nevertheless, the quantity $\dot{q}_k/|\mathbf{v}_k|$ (which relates to a ratio of the residence time and the reaction time, i.e., local Damkhöler number, at the reaction kernel [34]) decreased mildly, stayed nearly constant over a wide range, and as the flame lifted off the burner, decreased rapidly to a minimum level (3 to 4), which was comparable to the chemically passive agents. This result suggests that the reaction kernel shifted gradually downstream (where $\dot{q}_k/|\mathbf{v}_k| \approx$ constant) to seek a location where longer residence time is available for longer reaction time caused by agent addition (which lowers the overall reaction rate). A subtle balance between the residence time and the reaction time (or more specifically, the incoming flow velocity and the laminar flame speeds) must be important in flame stabilization [34]. As the flame lifted higher, it became more difficult to obtain the balance, thus leading to blowoff eventually.

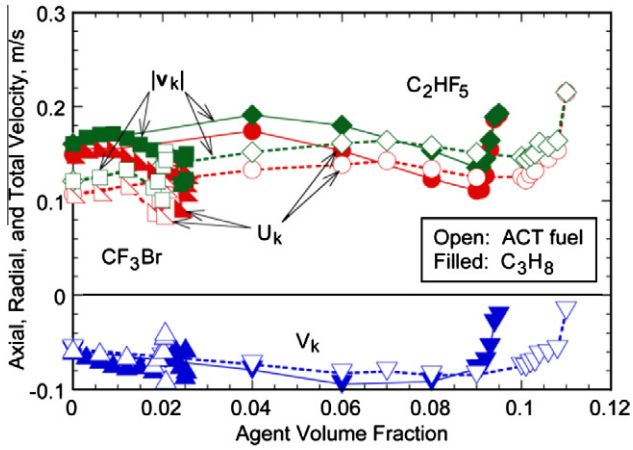

Fig. 9. Calculated axial (U_k) and radial (V_k) velocity components and total velocity ($|\mathbf{v}_k|$) at the reaction kernel of $0g_n$ propane and ACT fuel flames in air with added agent.

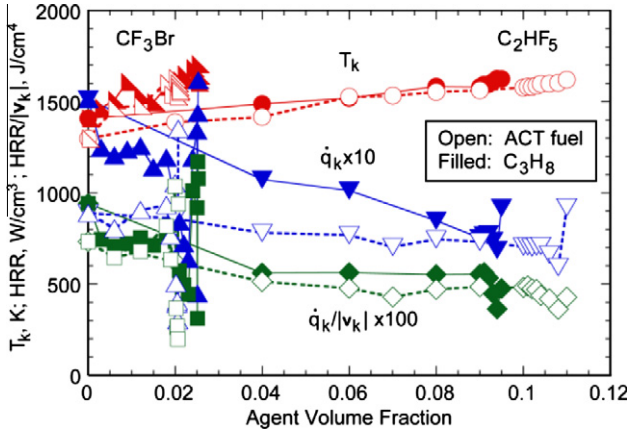

Fig. 10. Calculated heat-release rate, and its ratio to total velocity at the reaction kernel of $0g_n$ propane and ACT fuel flames in air with added agent.

3.3. Combustion enhancement

Figure 11 shows the maximum temperature in the trailing diffusion flame, the total heat-release rate ($\dot{q}_{\text{total}}$) integrated over the entire flame, and the flame base region ($\dot{q}_{<z_k+3\text{mm}}$) only. Unlike chemically passive agents [20,21], which work thermally to reduce the flame temperature by dilution, the maximum flame temperatures for both propane and the ACT fuel were nearly constant (≈1700 K) for C_2HF_5 or mildly increased for CF_3Br over an entire range of X_a varied until lifting. There was a striking difference between CF_3Br and C_2HF_5 in $\dot{q}_{\text{total}}$ over the entire flame. $\dot{q}_{\text{total}}$ decreased (i.e., inhibition) with added CF_3Br, whereas it increased (i.e., combustion enhancement) with added C_2HF_5, while for both fuels and both agents, $\dot{q}_{<z_k+3\text{mm}}$ was nearly constant. Thus, the combustion enhancement occurred only in the trailing flame. In fact, the heat release in the trailing flame ($\dot{q}_{\text{total}} - \dot{q}_{<z_k+3\text{mm}}$) doubled with added C_2HF_5 (at $X_a \approx 0.1$). Although the volumetric heat-release rate in the trailing flame was an order-of-magnitude smaller than the peak $\dot{q}_k$, integration over the entire trailing flame zone made the total value much larger. This result suggests the significant implication that even if the reaction kernel, with *premixed*-like flame structure, is weakened by halogenated agent addition toward the flame stability limit, the trailing *diffusion* flame can burn more reactants (including the agent itself) because of the additional heat release to form HF and CF_2O in the aforementioned "two-zone" flame structure. Although the global reaction and heat-release rates in $0g_n$ flames, reported in this paper, were generally small because of relatively slow diffusion-dominant transport processes, they could become

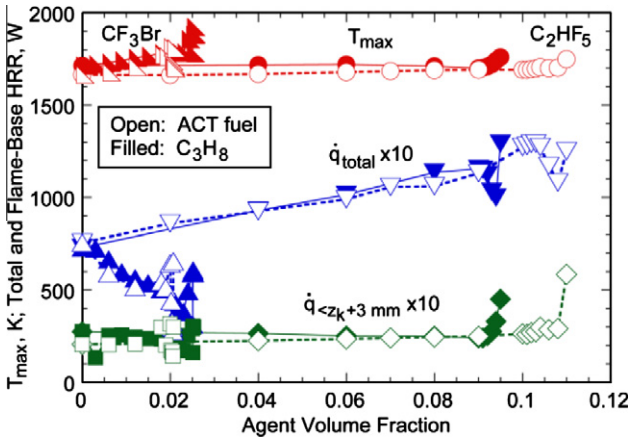

Fig. 11. Calculated maximum temperature, total heat release rate integrated over an entire flame, and the base region of $0g_n$ propane and ACT fuel flames in air with added agent.

orders-of-magnitude larger if convective transport would participate in the combustion processes.

4. Conclusions

Numerical simulations with full chemistry have revealed the effects of chemically active fire-extinguishing agents (CF_3Br and C_2HF_5) on the flame structure, blowoff mechanisms, and combustion inhibition or enhancement of propane and ACT fuel coflow diffusion flames in the cup-burner configuration. Absence of gravity uncovered previously unknown processes without complications induced by buoyancy in earth gravity. The flame tip opened due to local extinction by radiative heat losses when the calculated local flame temperature decreased to <1250 K. Addition of CF_3Br or C_2HF_5 to the oxidizer weakened the flame attachment point (reaction kernel) at the flame base, thereby inducing the detachment, lifting, and blowout extinguishment eventually. Unlike chemically passive agents studied previously, the calculated maximum flame temperature remained at nearly constant (≈1700 K) for C_2HF_5 or mildly increased for CF_3Br, while the reaction kernel temperature increased for both agents, as a result of additional heat release from the inhibitor itself. In the *premixed*-like reaction kernel, H_2O formed from hydrocarbon-O_2 combustion was converted further to HF and CF_2O by exothermic reactions, thus enhancing a heat-release rate peak. Nevertheless, CF_3Br successfully inhibited the reaction and reduced the overall total heat release. By contrast, the C_2HF_5 addition resulted in the combustion enhancement (increased total heat release), in the unique "two-zone" structure of the trailing *diffusion* flame, primarily by the HF formation in both inner and outer zones and the CF_2O formation in the outer zone.

Acknowledgment

This work was supported by The Boeing Company.

References

[1] J.W. Reinhardt, *Behavior of Bromotrifluoropropene and Pentafluoroethane When Subjected to a Simulated Aerosol Can, Explosion*, DOT/FAA/AR-TN04/4, 2004.
[2] J.W. Reinhardt, *Minimum Performance Standard for Aircraft Cargo Compartment Halon Replacement Fire Suppression Systems (2nd Update)*, DOT/FAA/AR-TN05/20, 2005.
[3] G.W. Gmurczyk, W.L. Grosshandler, *Proc. Combust. Inst.* 25 (1994) 1497–1503.
[4] Y.N. Shebeko, V.V. Azatyan, I.A. Bolodian, et al., *Combust. Flame* 121 (2000) 542–547.
[5] A. Suzuki, T. Inomata, H. Jinno, T. Moriwaki, *Bull. Chem. Soc. Jpn.* 6 (1991) 3345–3354.
[6] E. Ikeda, J.C. Mackie, *Int. J. Res. Phys. Chem. Chem. Phys.* 215 (2001) 997–1009.
[7] J.R. Mawhinney, B.Z. Dlugogorski, A.K. Kim, *A closer look at the fire extinguishing properties of water mist, in: Fire Safety Science – Proceedings of the Fourth International Symposium*, International Association for Fire, Safety Science, 1994.
[8] A. Hamins, K. McGrattan, G.P. Forney, *Unwanted Accelerated Burning After Suppressant Delivery, NIST SP-1004*, National Institute of Standards and Technology, Gaithersburg, MD, 2003.
[9] G. Holmstedt, P. Andersson, J. Andersson, *Investigation of scale effects on Halon and Halon alternatives regarding flame extinguishing, inerting concentration and thermal decomposition products, in: Fire Safety Science – Proceedings of the Fourth International Symposium*, International Association for Fire, Safety Science, 1994.
[10] V.R. Katta, F. Takahashi, G.T. Linteris, *Combust. Flame* 144 (2006) 645–661.
[11] G.T. Linteris, F. Takahashi, V.R. Katta, H. Chelliah, *Thermodynamic analysis of suppressant-*

enhanced overpressure in the FAA Aerosol Can Simulator, in: Fire Safety Science – Proceedings of the Tenth International Symposium, International Association for Fire, Safety Science, 2011.
[12] G.T. Linteris, D.R. Burgess, F. Takahashi, V.R. Katta, H.K. Chelliah, O. Meier, *Stirred-reactor calculations to understand unwanted combustion enhancement by potential Halon replacements*, *Combust. Flame* 159 (2012) 1016–1025.
[13] G.T. Linteris, L. Truett, *Combust. Flame* 105 (1996) 15–27.
[14] G.T. Linteris, D.R. Burgess, V. Babushok, M. Zachariah, W. Tsang, P. Westmoreland, *Combust. Flame* 113 (1998) 164–180.
[15] V.R. Katta, F. Takahashi, G.T. Linteris, *Combust. Flame* 137 (2004) 506–522.
[16] G.T. Linteris, V.R. Katta, F. Takahashi, *Combust. Flame* 138 (2004) 78–96.
[17] G.T. Linteris, F. Takahashi, V.R. Katta, *Combust. Flame* 149 (2007) 91–103.
[18] F. Takahashi, G.T. Linteris, V.R. Katta, *Proc. Combust. Inst.* 31 (2007) 1575–1582.
[19] F. Takahashi, G.T. Linteris, V.R. Katta, *Proc. Combust. Inst.* 31 (2007) 2721–2729.
[20] F. Takahashi, G.T. Linteris, V.R. Katta, *Combust. Flame* 155 (2008) 37–53.
[21] F. Takahashi, G.T. Linteris, V.R. Katta, *Proc. Combust. Inst.* 33 (2011) 2531–2538.
[22] V.R. Katta, L.P. Goss, W.M. Roquemore, *AIAA J.* 32 (1994) 84.
[23] W.M. Roquemore, V.R. Katta, *J. Vis.* 2 (2000) 257–272.
[24] H. Wang, X. You, K.W. Jucks, et al., USC Mech Version II. High-temperature combustion reaction model of $H_2/CO/C_1–C_4$ compounds, University of Southern California, Los Angeles, CA, 2007, available at <http://ignis.usc.edu/USC_Mech_II.htm>.
[25] D.A. Sheen, X.Q. You, H. Wang, T. Lovas, *Proc. Combust. Inst.* 32 (2009) 535–542.
[26] J. Li, A. Kazakov, F.L. Dryer, *J. Phys. Chem. A* 108 (2004) 7671–7680.
[27] J. Li, A. Kazakov, M. Chaos, F.L. Dryer, *Chemical Kinetics of Ethanol Oxidation*, US Sections/The Combustion Institute Meeting, 2007.
[28] J. Li, A. Kazakov, F.L. Dryer, *Int. J. Chem. Kinet.* 33 (2001) 859–867.
[29] V.I. Babushok, D.R.F. Burgess, W. Tsang, A.W. Miziolek, Simulation studies on the effects of flame retardants on combustion processes in a plug reactor, in: *Halon Replacements*, American Chemical Society, Washington DC, 1995, pp. 275–288.
[30] V.I. Babushok, T. Noto, D.R.F. Burgess, A. Hamins, W. Tsang, *Combust. Flame* 107 (1996) 351–367.
[31] D. Burgess, M.R. Zachariah, W. Tsang, P.R. Westmoreland, *Prog. Energy Combust. Sci.* 21 (1995) 453–529.
[32] D. Burgess, M.R. Zachariah, W. Tsang, P.R. Westmoreland, *Thermochemical and Chemical Kinetic Data for Fluorinated Hydrocarbons, NIST Technical Note 1412*, National Institute of Standards and Technology, Gaithersburg, MD, 1995.
[33] E.J.P. Zegers, B.A. Williams, E.M. Fisher, J.W. Fleming, R.S. Sheinson, *Combust. Flame* 121 (2000) 471–487.
[34] F. Takahashi, V.R. Katta, *Proc. Combust. Inst.* 28 (2000) 2071–2078.
[35] A. Hamins, G. Gmurczyk, W. Grosshandler, et al., Flame suppression effectiveness, in: W. Grosshandler, R.G. Gann, W.M. Pitts (Eds.), *Evaluation of Alternative In-Flight Fire Suppression for Full Scale Testing in Simulated Aircraft Engine Nacelles and Dry Bays*, NIST SP 861, National Institute of Standards and Technology, April 1994, pp. 345–465.
[36] T.A. Moore, A. Martinez, R.E. Tapscott, A comparison of the NMERI and ICI-style cup-burners, in: *Proceedings of the 7th Halon Options Technical Working Conference (HOTWC-97)*, 1997, pp. 388–395.
[37] G.T. Linteris, Flame suppression chemistry, in: R.G. Gann (Ed.), *Advanced Technology for Fire Suppression in Aircraft*, NIST Special Publication 1069, National Institute of Standards and Technology, 2007, pp. 119–338.
[38] A.G. Gaydon, H.G. Wolfhard, *Flames, their Structure, Radiation and Temperature*, fourth ed., Chapman and Hall, London, 1979, p. 168.
[39] F. Takahashi, V.R. Katta, *Proc. Combust. Inst.* 30 (2005) 375–382.